Preparation, Structure, and Properties of Copolyester-Ether Elastic Filaments

G. C. RICHESON and J. E. SPRUIELL, *Polymer Engineering Program, Department of Materials Science and Engineering and Center for Materials Processing, University of Tennessee, Knoxville, Knoxville, Tennessee 37996-2200*

Synopsis

Elastic filaments have been produced by melt spinning poly(tetramethylene terephthalate)/poly(tetramethylene ether glycol)-terephthalate (PTMT/PTMEG-T) copolymers of various hard segment contents (HSC). Some of these copolymers are difficult to spin because of their elastic nature and sluggish crystallization kinetics. Differential scanning calorimetry studies show that both the crystallization rate and temperature decrease as HSC decreases. When spinning into air, the filaments low in HSC do not crystallize on-line and are too tacky and soft to be taken up with a conventional constant tension winder. The elastic nature of these filaments prevents them from being taken up at speeds high enough for "stress-induced crystallization" to cause appreciable crystallization on-line. Spinning into a water bath allows the filaments to be taken up without a "sticking" problem. The microstructure and mechanical properties of the water-quenched filaments were found to be strongly dependent on composition and processing conditions. Small-angle and wide-angle x-ray techniques (SAXS and WAXD) indicate that the hard segment domains are lamellar-like crystallites which become preferentially oriented perpendicular to the fiber axis at high spin-draw ratios. As HSC decreases, the lamellae become more widely spaced. High levels of crystalline orientation can be produced using the water quench technique without creating appreciable levels of amorphous orientation. These are desirable features for obtaining high elastic recovery. Birefringence results indicate that these filaments continue to crystallize for up to 10 minutes after spinning. The relative degree of phase separation (DPS) decreases as HSC increases, but the actual level of crystallinity exhibits a maximum with respect to composition. Not coincidentally, the filaments that reach the highest crystallinity are the easiest to spin. The modulus of these filaments depends primarily on HSC and DPS, while the tenacity and ultimate elongation depend more on the degree of orientation developed during spinning. Elastic recovery increases as HSC decreases and as crystalline orientation increases.

INTRODUCTION

Thermoplastic elastomers (TPEs) are a new class of polymer which has been developed within the last 20 years. They exhibit characteristics of crosslinked elastomers but can be processed by conventional thermoplastic techniques.

Since TPEs combine the performance of rubber with the processing economy of thermoplastics, they have found wide acceptance in an area formerly dominated by crosslinked elastomers. As advances in polymer technology are made and new polymers with superior properties are developed, more opportunities are being found for their use in new applications and as replacements in existing applications. The copolyester-ethers are a part of this advancing technology. They have found widespread use as hose and tubing products, wire and cable insulation, and drive belts, as well as a number of molded products.

Journal of Applied Polymer Science, Vol. 41, 845–875 (1990)
 CCC 0021-8995/90/3-40845-31$04.00

The physical and mechanical properties of copolyester-ethers are determined to a large extent by their morphology. The degree of phase separation, total crystallinity, orientation of the chain segments, and the size and shape of crystalline domains, and their tendency to agglomerate into superstructures such as spherulites can vary widely depending on the composition and processing conditions used. In order to control the properties of the product, one must understand the relationships between materials, processing conditions, and microstructure.

Although a number of reports have dealt with the structure and properties of isotropic samples made by compression molding or casting techniques,[1-11] little attention has been given to the behavior of copolyester-ethers during processing operations which produce anisotropic or inhomogeneous samples such as extrusion, injection molding, or melt spinning.[11-14]

The primary goal of this research was to develop a better understanding of the processing–structure–property relationships in anisotropic copolyester-ether samples. In this work, a method was developed for melt-spinning elastic filaments from the copolyester-ethers. This required an understanding of the interaction of processing conditions and crystallization kinetics. Consequently, we describe the crystallization kinetics and their relationship to the processing procedures. The microstructures of the filaments were then studied as a function of composition and spinning conditions. The tensile and elastic properties of the filaments were determined and correlated with pertinent structural features. The insight gained by these studies provides fundamental information that may prove useful in understanding the behavior of these copolymers in other processes which produce anisotropic products, such as extrusion and coating operations or blow molding.

MATERIALS

The materials used in this study were supplied by E. I. du Pont de Nemours and Company. These copolymers consist of repeatedly alternating polyester and polyether blocks. The hard segment is a crystallizable polyester, poly(tetramethylene terephthalate) (PTMT), while the soft segment is made from poly(tetramethylene ether glycol) terephthalate (PTMEG-T).[4,15,16] The chemical structure of these copolymers is shown in Figure 1. The sequence lengths of the hard and soft segment blocks follow a geometric distribution since the synthesis involves equilibrium ester exchanges. The average hard segment block length and consequently the composition is controlled by selecting the mole ratio of reactants during polymerization.[3]

Four copolymers covering a wide range of compositions plus the hard segment homopolymer were investigated in this study. The compositions and approximate transition temperatures of the copolymer resins are shown in

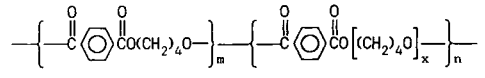

PTMT (HARD SEGMEMT) MW = 220 PTMEG-T (SOFT SEGMENT) MW ~ 1120

Fig. 1. The chemical structure of PTMT/PTMEG-T copolymers.

TABLE I
Composition and Approximate Phase Transition Temperatures of the Copolyester-Ethers Used in This Study

Polymer	Hard segment[a] wt-%	Average DP of hard segment[b]	T_m (°C)	T_g[c] (°C)
PTMT	100	> 150	221	+40
H7246	81	22	217	−18
H6346	75	17	202	−33
H5556	57	8	203	−55
H4056	44	6	152	−65
PTMEG[d]	0	—	38	−84

[a] *Source*: Ref. 15; L. W. Jelinski, F. C. Schilling, and F. A. Bovey, *Macromolecules*, **14**, 581–586 (1981).
[b] *Source*: Ref. 4.
[c] *Source*: Ref. 17.
[d] *Source*: Ref. 18.

Table I. The hard segment content that is reported is based on ^{13}C studies by Jelinski et al.[16] and Bovey.[15] The average degree of polymerization (DP) of the hard segment was estimated from the data of Cella.[4] Glass transition temperatures were estimated from the data of Van Bogart et al.[17] It should be noted that T_g varies with the DPS, and thus varies to some extent with the thermal history of the sample. The PTMEG data were reported by Wetton and Allen.[18] The melting temperatures of the copolymers were determined by the authors, and represent the temperature at the peak maximum.

CHARACTERIZATION TECHNIQUES

The copolyester-ether filaments prepared in this research were characterized by a number of techniques. In some of the techniques, it was necessary to introduce approximations and modifications in the analysis in order to proceed with the research. Descriptions of the experimental techniques are given below.

Crystalline Orientation Functions

Crystallite orientation functions were determined using a Rigaku x-ray diffractometer (D/MAX-IA) equipped with a digital PDP 11/34 computer. Intensity measurements were made in symmetric transmission mode. Monochromatic CuK_α radiation was obtained using a diffracted beam monochromator.

Since the PTMT crystals are triclinic, a minimum of three ($hk0$) planes are necessary for a rigorous determination of the chain axis orientation. Only two suitable ($hk0$) planes are available, however; namely the (100) and the (010). Following the method of Yoshihara et al,[19] a new unit cell is defined such that the angle between the new lattice vectors **a**′ and **b**′ is 90°. This orthorhombic approximation allows an equation to be derived relating the chain axis orientation, $f_{c,Z}$, to $\langle \cos^2 \phi_{100,Z} \rangle$ and $\langle \cos^2 \phi_{010,Z} \rangle$, where Z is the reference

direction and ϕ is the angle between the normal to the diffraction plane and reference direction.

Yoshihara's equation, originally derived for poly(ethylene terephthalate), has the form

$$f_{c,z} = 2\frac{f_{100,z}\cos(2\eta_{010}) - f_{010,z}\cos(2\eta_{100})}{\cos(2\eta_{100}) - \cos(2\eta_{010})} \tag{1}$$

where

$$f_{i,z} = \frac{3\langle\cos^2\phi_{i,z}\rangle - 1}{2} \tag{2}$$

and η_j are the angles between the reciprocal lattice vectors (**a*** and **b***) of the paratropic planes and the b' axis. This same equation can be applied to PTMT once the proper values of η_j are determined. The angles in PTMT between the original reciprocal lattice vectors and the a' and b' axes are summarized below:

	a'	b'
a*	85.6°	4.4°
b*	24.3°	65.7°

Substituting in the values of η_j results in the following equation:

$$f_{c,z} = \frac{1.976f_{100,z} + 1.322f_{010,z}}{-1.65} \tag{3}$$

Small Angle X-ray Scattering (SAXS)

The SAXS data were obtained using the National Center for Small Angle Scattering Research (NCSASR) 10-m x-ray facilities at the Oak Ridge National Laboratory (ORNL). The two-dimensional position-sensitive detector in this system is particularly useful for acquiring quantitative intensity data on anisotropic samples. For investigations of sample morphology and determinations of the degree of phase separation, a sample-to-detector distance of 2.126 meters was used. This provides an angular range of detection from 2.8 mrad to 49 mrad with CuK_α radiation, corresponding to structures in the range of approximately 5 to 300 Å.

At 40 keV and 50 mA, exposure times of 30 minutes to 2 hours were required to produce adequate count statistics. Raw data were corrected for instrumental scattering (due mostly to diffraction from the collimation slits), "dark current" in the detector due to cosmic radiation and electronic noise, detector dead time, and detector sensitivity. NCSASR software was used for data manipulation and graphics.

Long Period. If there is discrete scattering, the long period L can be calculated from the maximum in the intensity distribution $I(s)$ using Bragg's law:

$$L = 1/s \tag{4}$$

where $s = 2(\sin\theta)/\lambda$.

Determination of the Degree of Phase Separation. For an isotropic system with pinhole collimation, the invariant has the form $Q = 4\pi\int s^2 I_a(s)ds$.[20] For an anisotropic system in which the scattered intensity is cylindrically symmetric about s_1 (the fiber axis in this case), the invariant takes the form[21]:

$$Q = 4\pi\int_0^\infty\int_0^\infty I_a(s_1, s_2)s_2\, ds_1\, ds_2 \tag{5}$$

The mean square electron density fluctuation defined as $\langle\eta^2\rangle \equiv \overline{(\rho - \bar{\rho})^2}$ may then be determined from the invariant

$$\overline{(\rho - \bar{\rho})^2} = \frac{4\pi}{\nu\tau}\int_0^\infty\int_0^\infty I_a(s_1, s_2)s_2\, ds_1\, ds_2 \quad \text{(anisotropic case)} \tag{6}$$

where ρ = electron density in $e^-/\text{Å}^3$, $\bar{\rho}$ = average electron density, $\nu = \lambda^2 i_e$, i_e = Thompson scattering constant of a free electron ($7.92 \times 10^{-26}\text{cm}^2$), N = Avogrado's number (6.023×10^{23}/mol), I_a = scattered intensity in absolute units (I/P_0), P_0 = intensity of the primary beam, $s = 2(\sin\theta)/\lambda$, s_1 = scattering vector in direction 1 (fiber axis), s_2 = scattering vector in direction 2 (perpendicular to the fiber axis), $\tau = d\bar{\rho}N$ (electrons/cm^2), and d = sample thickness, in cm.

This mean square electron density fluctuation can be used to quantitatively characterize the DPS in a two-phase system. For an ideal two-phase system (sharp domain boundaries and uniform electron density within the domain) with known electron densities, ρ_1 and ρ_2, the volume fraction ϕ_1 and ϕ_2 of each phase can be determined from

$$\langle\eta^2\rangle \equiv \overline{(\rho - \bar{\rho})^2} = \phi_1\phi_2(\rho_1 - \rho_2)^2 \tag{7}$$

Applications of this principle to real (nonideal) systems having diffuse phase boundaries and mixing within the phases have been discussed by Bonart and Müller[22] and Koberstein and Stein.[23] In the copolyester-ether system, the parameter η is not a unique determination of the degree of phase separation since η depends on the total hard segment content as well as the degree of phase separation. Also, since the amorphous phase is a mixture of polyether segments and amorphous polyester sequences, the electron density of this phase changes as the DPS changes. This increases the value of η due to an increase in both the $\phi(1 - \phi)$ and $(\rho_1 - \rho_2)$ terms.

In order to get around some of these difficulties Bonart and Müller[22] defined an index ϵ which is the ratio of the experimentally observed electron density fluctuation $\langle\eta^2\rangle$ to the theoretical value calculated for a given composition assuming total and ideal phase separation $\langle\eta_0^2\rangle$:

$$\epsilon = \langle\eta^2\rangle/\langle\eta_0^2\rangle \tag{8}$$

The quantity ϵ is not a rigorous determination of the DPS but provides a useful means for comparing the relative degree of phase separation among samples of the same or different compositions.

Thermal Analysis

The crystallization kinetics and melting behavior of the copolymer resins were studied using a Perkin-Elmer DSC-2 differential scanning calorimeter (DSC). Subsequent thermal analysis on resins and spun filaments were carried out using a Perkin-Elmer DSC-7. Liquid nitrogen was used to cool the sample chamber during subambient studies. The use of DSC scans to determine crystallinity or morphological features must be done with caution since PTMT and the copolymers crystallize during the scan. The scans may not be representative of the materials at room temperature. A discussion of these problems and an interpretation of the multiple melting behavior of the copolyester-ethers have been presented by Stevenson and Cooper.[24]

Birefringence

Fiber diameter d and retardation Γ measurements were made using an Olympus microscope and a 30λ Berek compensator. The diameters were calibrated by means of an Olympus graduated slide marked off in 0.02 mm increments. The birefringence Δ_{tot} is calculated as follows:

$$\Delta_{tot} = \Gamma/d \tag{9}$$

Density

The density of the copolymer resins and filaments were measured using a conventional density gradient column prepared from sodium bromide and water. The column was calibrated using glass beads of accurately known densities.

In theory, the degree of crystallinity can be calculated from the measured density ρ_{tot}, using the additivity of specific volumes and by assuming ideal mixing in the amorphous phase:

$$\frac{1}{\rho_{tot}} = \frac{w_c\omega_1}{\rho_c} + \frac{(1 - w_c)\omega_1}{\rho_{a1}} + \frac{(1 - \omega_1)}{\rho_{a2}} \tag{10}$$

where the subscripts 1 and 2 refer to the PTMT and PTMEG-T components, respectively, and c and a refer to the crystalline and amorphous phases, respectively. "ω_1" is the weight fraction of the hard segments in the copolymer and "w_c" is the weight fraction of PTMT segments that are crystalline. Assuming $\bar{x} = 12$ (see Bovey[15]) in the chemical formula, an amorphous density (ρ_{a2}) of 1.033 g/cm^3 is obtained for amorphous PTMEG-T. Crystalline PTMT has a density of 1.396 g/cm^2, while amorphous PTMT has a density of 1.282 g/cm^3. Using the values of HSC (ω_1) given in Table I and the measured density, the degree of phase separation w_c can be calculated. The

degree of crystallinity x_c is then simply the product of the HSC and the DPS:

$$x_c = w_c \omega_1 \tag{11}$$

Dynamic Mechanical Data

An Imass Autovibron® dynamic viscoelastometer was used to determine the glass transition temperatures of selected filaments. This instrument is equipped with a Hewlett-Packard 6940B multiprogrammer for automatic temperature control and data aquisition. A nitrogen purge gas run through a liquid nitrogen bath was used to cool the sample chamber to subambient temperatures. Data were taken at approximately 1° intervals from −100°C to about 100 or 150°C depending on the composition. Data were obtained at three frequencies: 1.1, 11, and 110 Hz. The loss factor (tan δ) was calculated as a function of temperature. The maximum in the tan δ curve was taken as the glass transition temperature.

Shrinkage in Boiling Water

The shrinkage of oriented filaments during free annealing is often associated with orientation relaxation in the amorphous phase. The amount of shrinkage is a complex function of the state of amorphous orientation, relaxation time and the crystallization behavior. Nevertheless, shrinkage provides valuable information about the filaments. A high level of shrinkage can be attributed to contraction of amorphous chains. Low shrinkage may mean that either there is little amorphous orientation or that the sample has a high level of crystallinity which prevents shrinkage. Careful interpretation of the results is required to provide meaningful information in the latter case.

The amount of shrinkage (S) is defined as the length before annealing (l_0) minus the length after annealing (l), divided by the original length:

$$\%S = \frac{l_0 - l}{l_0} \times 100\% \tag{12}$$

Filaments approximately 300 mm long were placed in boiling water for 2 minutes (i.e., annealed at 100°C). The filaments were then removed and allowed to cool to room temperature. The lengths before and after annealing were used to calculate the amount of shrinkage.

Mechanical Properties

Tensile Properties. The mechanical properties of the filaments were measured using an Instron tensile tester (Table Model 1122). A short gage length was necessary because of the large elongations to break in some of the more elastic filaments and the limited amount of travel of the crosshead. A gage length of 30 mm and a crosshead speed of 50 mm/min were selected, giving

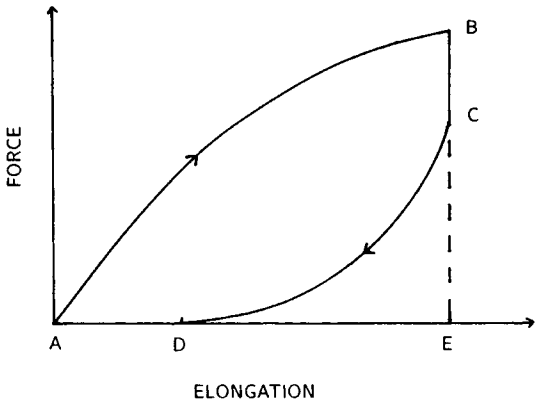

Fig. 2. Schematic diagram showing how stain recovery and work recovery are calculated from cyclic stress–strain curves.

an initial elongation rate of 167%/min. The elongation was determined from the distance the crosshead had traveled at any given time during the test.

Young's modulus, the elongation to break, and the breaking stress (tenacity) of the filaments were determined from the force-time curves obtained. The modulus was determined from the slope of the initial portion of the curve. The tenacity was defined as the maximum load sustained by the filaments divided by the original cross-sectional area.

Elastic Properties. In order to quantitatively investigate the elastic properties, the filaments were subjected to cyclic testing on the Instron tensile tester. The filaments were stretched to a given preselected elongation and allowed to relax for 30 seconds before reversing the crosshead and allowing the filament to retract to zero stress. The samples were again allowed to relax for 30 seconds and the cycle was repeated at a higher elongation. The stress at strains higher than those previously reached is fairly independent of the strain history as has been previously shown by Lilaonitkul et al.[6] The composite stress–strain curve from cyclic testing is almost identical to a curve produced by a single stretch to the final strain. For this reason, the total work recovery from a given elongation can be calculated from the composite extension curve and the retraction curve as shown in Figure 2. The values calculated in this manner are insensitive to step size and are comparable to the values that would be obtained if the sample had been stretched to those elongations in a single step.

QUIESCENT CRYSTALLIZATION BEHAVIOR

Before trying to melt-spin filaments from these copolymers, the crystallization kinetics under quiescent, isothermal conditions were studied as well as the crystallization behavior while cooling at constant rate. This provides basic information on the nature of the crystallization behavior and the relative

TABLE II
Crystallization Half-times, Avrami Exponents, and Crystallization Rate Constants

	T_c (°C)	$t_{1/2}$(min)	n	K (min^{-n})
H4056	84.0	2.67	3.89	0.0152
	90.0	3.36	3.81	0.00685
	94.0	3.99	3.66	0.00438
	98.0	4.57	3.60	0.00293
	104.0	5.76	2.90	0.00432
	112.0	11.76	2.97	0.000459
H5556	155.0	3.62	3.39	0.00885
	159.0	5.35	3.09	0.00389
	163.0	7.46	3.17	0.00119
	165.0	8.63	2.96	0.00118
	169.0	16.75	2.39	0.000823
H6346	155.0	2.98	3.22	0.0206
	159.0	4.49	3.03	0.00732
	161.0	5.56	2.98	0.00417
	163.0	7.10	—	—
	165.0	9.00	3.04	0.000871
	167.0	9.69	2.72	0.00144
H7246	174.5	1.89	3.25	0.0876
	180.5	4.46	2.97	0.00817
	182.5	5.27	2.62	0.00891
	184.5	6.17	2.94	0.00329
	186.5	7.29	3.05	0.00162
	188.5	7.29	3.05	0.00162
PTMT	188.2	2.93	2.83	0.0331
	191.2	3.76	2.79	0.0172
	192.7	4.78	2.61	0.0117
	194.2	5.67	2.66	0.00686
	195.7	5.96	—	—
	197.2	8.55	2.31	0.00488
	199.8	13.8	—	—

crystallization rates of the various compositions. Comparison of these results to commercially spun materials such as poly(ethylene terephthalate) and polypropylene were useful in determining what sort of spinline behavior to expect from the copolymers.

Isothermal Crystallization

Samples of 10–15 mg were melted in the DSC at temperatures about 25°C above their highest melting point for 5 min to eliminate all traces of crystallinity. The samples were then rapidly cooled to the desired crystallization temperature and allowed to crystallize isothermally. Temperatures were selected such that the transformation occurred within 2–30 min. The crystallization temperatures are given in Table II and typical curves showing the relative crystallinity, x_t/x_∞, as a function of $\ln t$ are shown in Figure 3. Half-times, $t_{1/2}$, determined from such curves are given in Table II for each composition and crystallization temperature.

The crystallization rate is of primary importance in this study. Table II shows that the *temperature* at which the half-times are in the 2–15 min range *decreases* rapidly as hard segment content *decreases*. A plot of the half-time

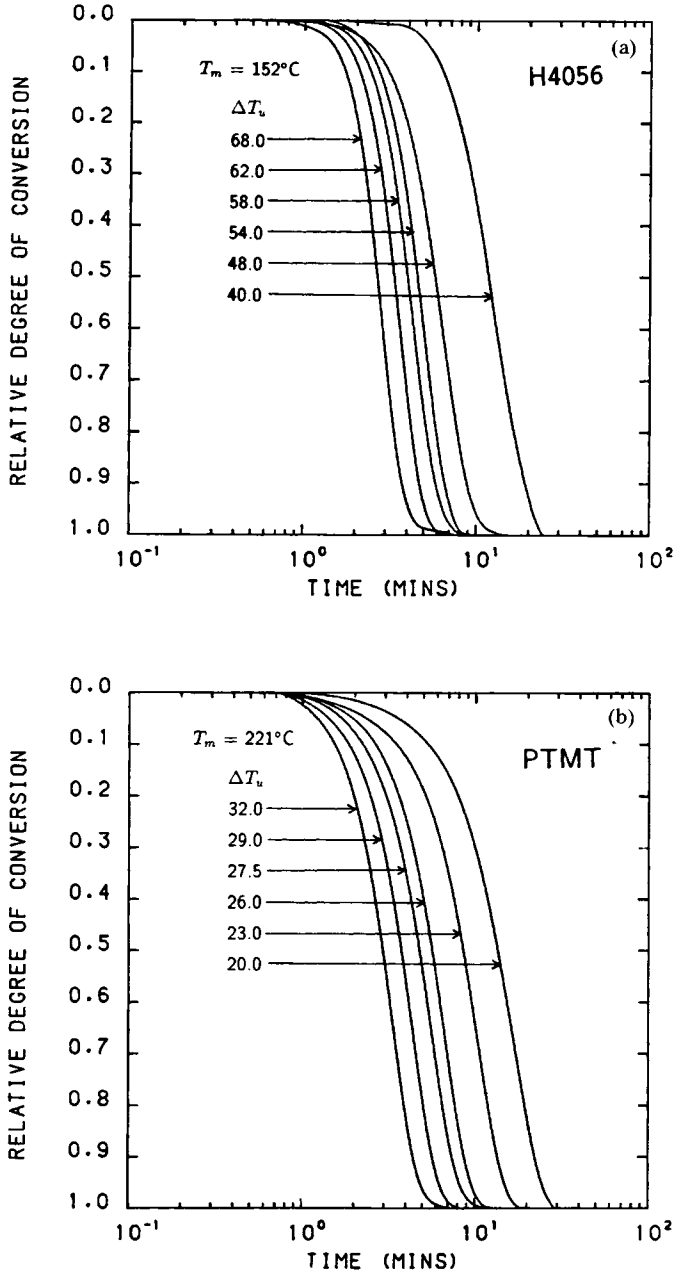

Fig. 3. Relative degree of conversion as a function of time for (a) H4056 and (b) PTMT.

of crystallization as a function of supercooling and composition is shown in Figure 4. As hard segment content (HSC) is reduced, the crystallization rate decreases and much higher degrees of supercooling are required for crystallization. The H4056 composition crystallizes even more slowly than poly(ethylene terephthalate) (PET), which is considered to have sluggish crystallization kinetics.

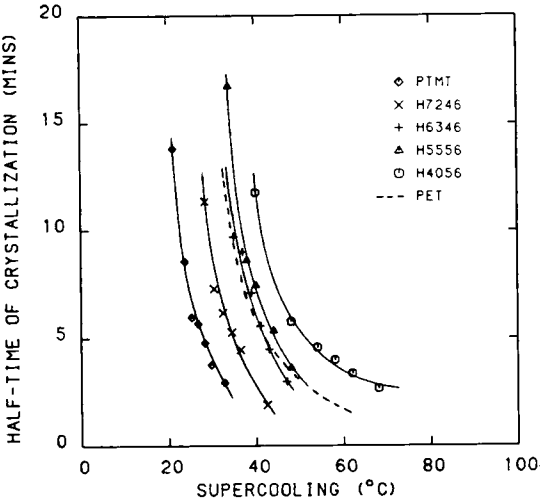

Fig. 4. Half-times of crystallization as a function of the degree of undercooling for the copolyesters. The results for PET are shown for comparison.

The data were further interpreted with the aid of the Avrami equation,[25] which for polymers can be expressed as:

$$\frac{x_t}{x_\infty} = 1 - \exp(Kt^n) \tag{13}$$

The Avrami exponent "n" can be determined from a plot of $\ln(-\ln(1 - x(t)))$ versus $\ln(t)$. This should yield a straight line with slope "n" and intercept "K". The values of "n" obtained in this way are given in Table II. The value of "n" increases as HSC and degree of supercooling decrease. The value of "K" is very sensitive to the slope of the line in the plot of $\ln(-\ln(1 - x(t)))$ versus $\ln(t)$. It may be better to determine "K" using the half-time of crystallization data. Substituting 0.5 for the relative degree of conversion in Eq. (11) leads to:

$$K = \ln 2/(t_{1/2})^n \tag{14}$$

Using the values of "n" and the half-times of crystallization, $t_{1/2}$, the values of "K" can be determined. These are reported in Table II.

Nonisothermal Crystallization

Studies of the crystallization behavior while cooling at constant rate show that the crystallization temperature drops with decreasing HSC and increasing cooling rate (see Fig. 5). At the higher cooling rates, the compositions high in HSC crystallize well above room temperature (> 90°C), while the H4056 composition must cool to almost 25°C before it crystallizes.

Crystallization from the Glassy State

Since the copolymers are above their respective glass transition temperatures at room temperature, it may be possible for melt-spun filaments to

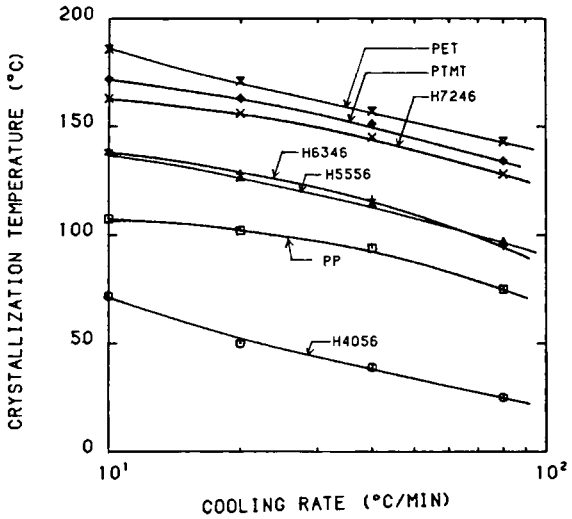

Fig. 5. Crystallization temperature of the copolyester-ethers as a function of composition and cooling rate. Polypropylene (PP) and poly(ethylene terephthalate) (PET) are shown for comparison.

crystallize after spinning. In order to study the crystallization behavior of these copolymers from the glassy state, samples were quenched from the melt in liquid nitrogen. The samples produced in this manner were clear. Samples were then transferred in liquid nitrogen to the DSC, which was being held at -100°C. Heating at 5 or 10°C/min, produced a crystallization exotherm. In H4056, it occurred at about -12°C. As shown in Figure 6, the crystallization temperature increases as HSC increases. The copolymer highest in HSC

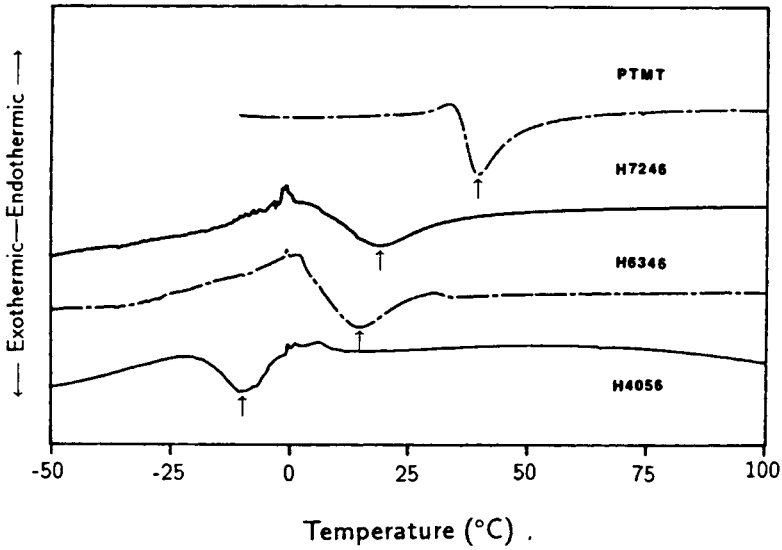

Fig. 6. DSC curves showing crystallization from the glassy state. The crystallization peaks for H4056, H6346, H7246, and PTMT are at -12, 14, 18, and 40°C, respectively.

crystallizes at about 18°C, while the PTMT homopolymer crystallizes at about 40°C. It is evident from this experiment that crystallization can take place at room temperature in all the copolymers. Pure PTMT is below its T_g at 25°C and does not crystallize from the glassy state at this temperature.

Discussion of Quiescent Crystallization Behavior

The isothermal crystallization studies show that the crystallization rate decreases with decreasing hard segment content at a given degree of supercooling. As HSC decreases, higher degrees of supercooling are required before crystallization takes place. The H4056 composition crystallizes even more slowly than poly(ethylene terephthalate)(PET), which is considered to have sluggish crystallization kinetics. Since PET crystallizes in the spinline only under conditions of high stress, the compositions low in HSC may not crystallize in the spinline.

Zhu et al.[26] found that spherulitic structures were produced by isothermal crystallization of copolyester-ethers at low degrees of supercooling. As the supercooling was increased, the nucleation density increased dramatically. Zhu and Wegner[14] found that the morphology changed from spherulitic in samples crystallized isothermally to a continuous network of lamellae in samples quenched rapidly to room temperature from the melt.

The values of "n" calculated with the aid of the Avrami equation indicate that the crystalline growth is approximately three-dimensional in all compositions during quiescent, isothermal crystallization at low degrees of supercooling. The values of "n" were found to increase slightly as HSC and degree of supercooling decreased. These results are in contrast to those obtained by Zhu and Wegner.[14] The values of "n" they report do not change appreciably with degree of supercooling. The noninteger values of "n" are attributed to the nongeometrical shape of the growing crystals.

The nonisothermal crystallization studies show that the crystallization temperature drops with decreasing HSC and increasing cooling rate. The H4056 composition was near room temperature before crystallization started. These results suggest that crystallization will not occur in the spinline during melt spinning of samples low in HSC.

Copolymer samples quenched in liquid nitrogen are able to partially crystallize at temperatures below 25°C because of their low glass transition temperatures. Thus, filaments which do not crystallize in the spinline may still crystallize after take-up.

Briber and Thomas[2] found that after cooling isothermally crystallized copolyester-ether samples to room temperature, some of the hard segment sequences remaining in the matrix crystallized. This new growth was found to form at the edge of existing crystallites or as smaller crystallites scattered through the matrix. The new crystallites took weeks to form at room temperature. These results imply that fractionation according to sequence length can occur. The authors explain that the fractionation occurs not as a result of incompatibility, but due to a coupling of the sequence length with the stable crystallite size at a given crystallization temperature. Thus, shorter segments can crystallize at low temperatures, albeit at very slow rates.

The samples produced by quenching in liquid nitrogen were clear. Films produced by Zhu and Wegner[14] by rapid quenching from the melt were also clear. Upon annealing, their samples remained clear, indicating that the nucleation density was very high and that crystallites much smaller than the wavelength of light were produced.

The various aspects of crystallization behavior discussed above are useful in understanding how the structure develops in the melt spun filaments.

FIBER FORMATION AND HEAT TREATMENT

Melt-Spinning Techniques

The filaments were produced by melt spinning from a Fourné screw extruder equipped with a Zenith metering pump. Several different take-up methods were tried. The PTMT homopolymer and copolymers having a high hard segment content (H7246 and H6346) can be spun easily in air. However, the sluggish crystallization kinetics of the compositions low in HSC caused sticking and stretching problems during take-up using this method. H4056 did not crystallize at all in the spinline and could not be taken up on the winder. In order to solidify the filaments faster and eliminate the sticking problems, a water quench bath was used. The bath was equipped with motorized rollers to prevent stretching of the filament between the bath and the constant tension take-up device. This apparatus is shown in Figure 7. The water bath was kept at 26.5 $\pm$ 1.5°C. After much experimentation, the air gap was set at 16 $\pm$ 1 cm to minimize draw resonance and melt instability. A polyester carrier yarn introduced into the spinline at the second godet prevented the copolyester filament from drawing in the winding device. With this set-up, all compositions could be spun under controlled and reproducible conditions. Filaments could

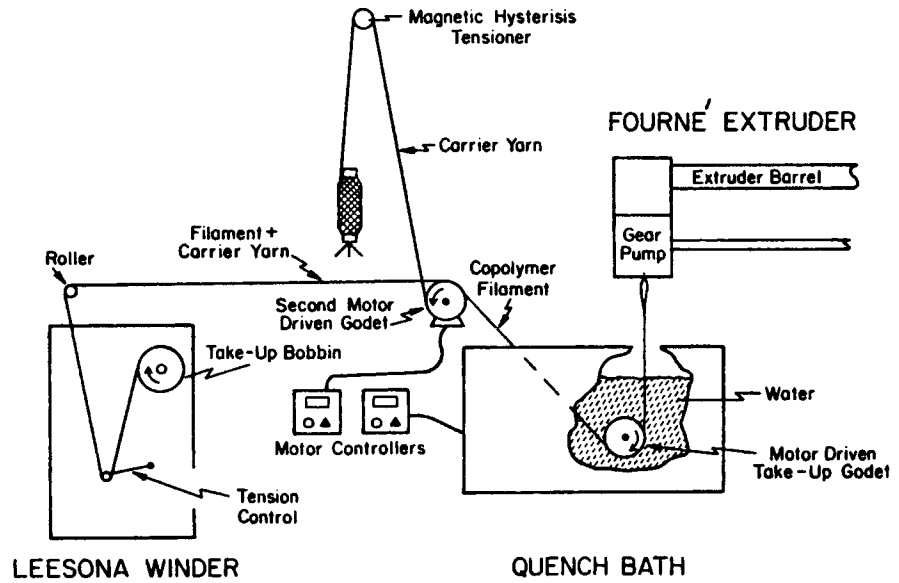

Fig. 7. Schematic diagram of the spinline, water bath, and winder.

be taken up at speeds up to 275 to 450 m/min depending upon the composition.

Crystallization Behavior During Spinning

During spinning without a quench bath, the filaments become increasingly tacky and difficult to handle as HSC decreases. This is easily explained by the crystallization kinetics of the copolymers from the melt. The amount of time and the degree of supercooling required for crystallization increases as HSC decreases.

Pure PTMT filaments with a quench bath present no problem to spinning. Although density measurements indicate they are amorphous, they are below their T_g and are quite strong. Of the copolymers, the H5556 filaments are the easiest to handle, followed by the H7246 and H6346 filaments. H4056 is the most difficult to take-up. It stretches quite easily in a taffy-like manner and a carrier yarn must be used to prevent it from drawing in the winder.

In order to investigate this interesting behavior further, filaments were spun from an Instron capillary rheometer into a water bath, and the birefringence was measured as a function of *time after initial contact with the water*. The birefringence corresponding to an elapsed time of 3 seconds could be obtained by measuring the retardation on-line just as the filament emerged from the bath. The filament was then quickly cut and subsequent measurements were made off-line. An increase in birefringence can be attributed to an increase in molecular orientation in the sample. Crystallization can produce such an increase when it occurs from an oriented melt due to oriented nucleation and subsequent growth of these oriented nuclei.

The results of this experiment are shown in Figure 8. H5556 has appreciable birefringence coming out of the bath. Little or no change in birefringence occurs after spinning. It is believed that considerable phase separation has already taken place in the bath and that little or no further crystallization takes place at room temperature. The birefringence of the H7246 and H6346 filaments is high emerging from the bath, and continues to increase slowly for

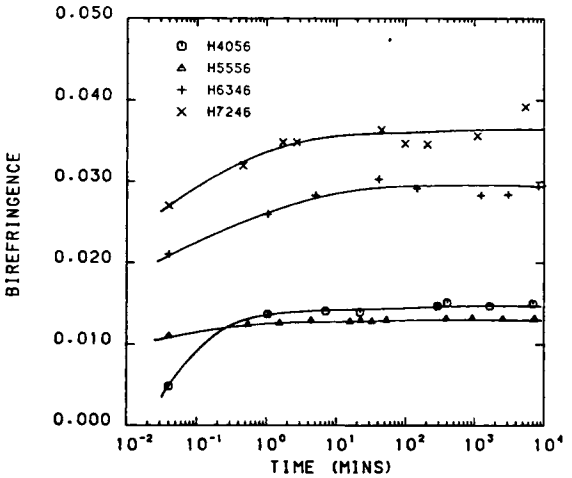

Fig. 8. Birefringence of the water quenched filaments as a function of time.

several minutes. This indicates that these compositions partially crystallize in the bath and that further crystallization takes place during or after take-up. The birefringence of H4056 is fairly low coming out of the bath, but it increases sharply during the first minute and then more slowly for several more minutes. This indicates that little crystallization takes place in H4056 during spinning. Most crystallization occurs while the filament is being taken up or after it is on the bobbin. Quick cooling to room temperature and the small amount of crystallization that takes place during take-up, keeps the filaments from sticking together on the bobbin.

Equatorial WAXD scans of the spun fibers taken immediately after spinning show that little or no additional primary crystallization occurs after the first 10 minutes, but that some secondary growth or crystallite perfection may take place. This effect is most pronounced for H4056.

The crystallization kinetics of these copolymers from the oriented rubbery state are not well understood. Apart from orientation effects, two factors would seem to control the crystallization behavior. The maximum crystallization rate in the range of temperatures from T_g to T_m is determined by the composition and the sequence length distribution. For a given composition, the crystallization rate at a particular temperature is greatly influenced by the proximity of the sample temperature to the optimum crystallization temperature for that composition. The degree of supercooling experienced by the filament during crystallization may determine the maximum degree of crystallinity that can be achieved at that temperature.

Filaments spun from the PTMT homopolymer are apparently quenched to a temperature below their T_g (40°C) so rapidly that there is not enough time for appreciable crystallization to take place during cooling. Since the copolymers are quenched under similar conditions, one would expect little or no crystallization to occur until they are at or near the quench temperature ($\sim$ 26°C). (Remember that the crystallization rate and optimum temperature drop as HSC decreases.) The H5556, H6346, and H7246 compositions all crystallize fairly rapidly at temperatures close to the quench temperature judging by the significant levels of birefringence they exhibit upon emergence from the water bath. Crystallization of the H5556 filament seem to have stopped by the time it emerges from the bath, while the H7246 and H6346 filaments continue to crystallize for several more minutes. It may be that H5556 is closer to its optimum crystallization temperature than either H7246 and H6346 and crystallizes more rapidly in the bath. The sluggish crystallization kinetics of the H4056 composition allows relatively little crystallization to occur in the bath, but since this copolymer is well above T_g at room temperature, it continues to crystallize after spinning.

STRUCTURE OF MELT-SPUN FILAMENTS

Before characterization, these filaments were conditioned at room temperature for several months. The microstructure of the various filaments were characterized using birefringence, density, DSC, rheovibron, WAXD, and SAXS techniques. The degree of orientation, degree of phase separation, and details of the morphology were determined as a function of composition and spin-draw ratio (SDR).

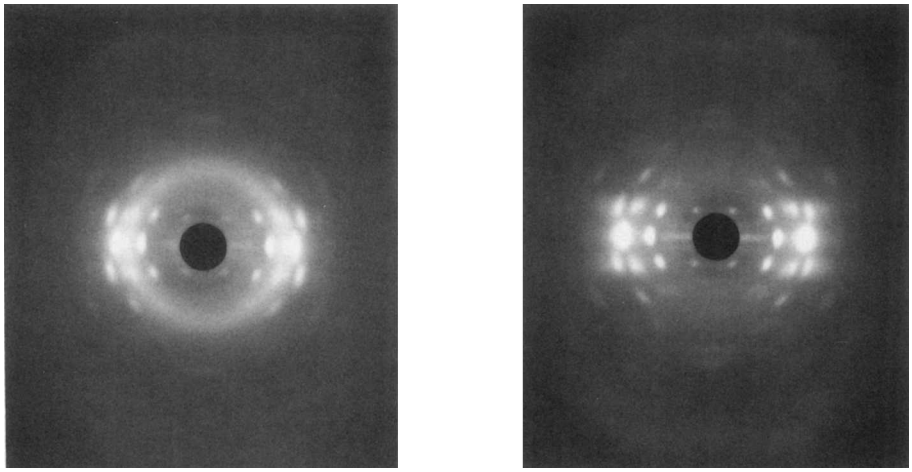

Fig. 9. WAXD patterns of highly oriented filaments of (a) H4056 and (b) PTMT. The copolymer pattern is very similar to that of the homopolymer. There does not appear to be a crystalline PTMEG phase in H4056.

General Structure and Morphological Features

WAXD patterns of all the copolymers show a diffuse halo from the amorphous phase and diffraction peaks that correspond to PTMT crystallites. WAXD patterns of drawn H4056 and PTMT filaments are compared in Figure 9. The only difference between the patterns of the two materials is the strong amorphous halo that appears in the H4056 pattern. There is no evidence of a crystalline PTMEG-T phase in any of the compositions studied.

Rheovibron curves of the copolymers, shown in Figure 10, exhibit a single, broad glass transition region that is intermediate to the glass transition temperatures of the two homopolymers. The broad transition region is believed to be a result of the broad distribution of hard segment sequence lengths and slight inhomogeneities in the amorphous phase. Two separate peaks would be expected if there were an amorphous PTMT phase in addition to the amorphous PTMEG-T phase. Thus, within our limits of detection, one phase is made up entirely of crystalline PTMT segments, while the other phase consists of the remaining uncrystallized PTMT segments and all of the PTMEG-T segments.

Small-angle x-ray scattering patterns of as-spun and conditioned H4056 and H7246 filaments are shown in Figure 11. Two main features should be noted. First, the two-point patterns indicate a lamellar structure with some degree of preferred orientation. As SDR is increased, the lamellae become increasingly aligned with their long axis perpendicular to the fiber axis. Second, the intensity of the peaks increases as HSC decreases. This suggests there may be an increase in the mean square electron density difference of the phases as HSC decreases. As discussed earlier, this can result from changes in either the

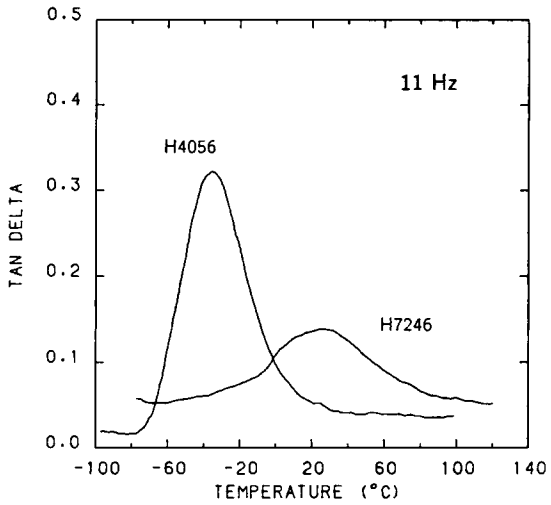

Fig. 10. Results of dynamic mechanical testing on H4056 and H7246 filaments.

volume fraction of each phase or the electron density difference between the phases or both. These results will be analyzed more quantitatively in a subsequent section. In as-spun filaments, the long period is virtually independent of SDR, although it increases substantially with decreasing HSC as shown in Figure 12.

Orientation

A high level of crystalline orientation is desired for maximum strength and elasticity.[12] The birefringence of these filaments increases with SDR, as shown

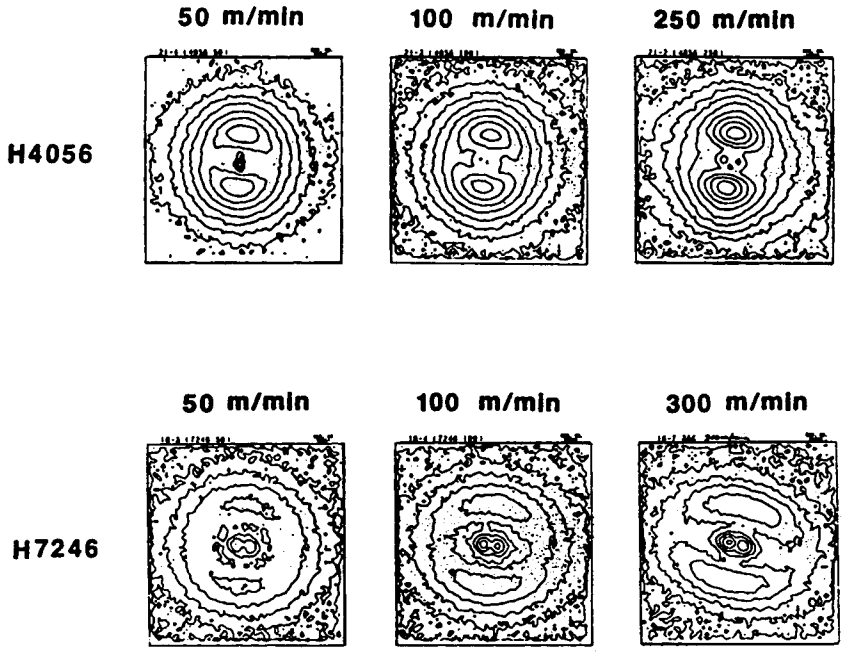

Fig. 11. SAXS patterns of H4056 and H7246 filaments at different take-up speeds.

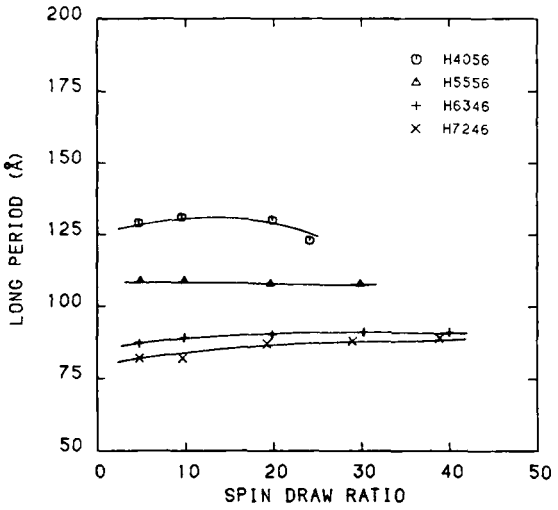

Fig. 12. Long period of the as-spun filaments as a function of spin draw ratio.

in Figure 13. The birefringence also generally increases with HSC in the copolymers, except that the PTMT homopolymer exhibits a lower birefringence than any of the copolymers. This appears to be due to the fact that the as-spun homopolymer filament has not crystallized. Crystallization from oriented nuclei has occurred in the copolymers, resulting in a higher birefringence. As shown in Figure 14, WAXD techniques indicate that the degree of preferred orientation of the crystalline hard segments increases rapidly up to a point as spin draw ration (SDR) increases, and then levels off. Since the chain axes of the crystalline hard segments are preferentially aligned parallel to the fiber axis at high SDRs, while the lamellae are aligned perpendicular to the fiber axis, the chain stems must traverse the short dimension of the lamellae.

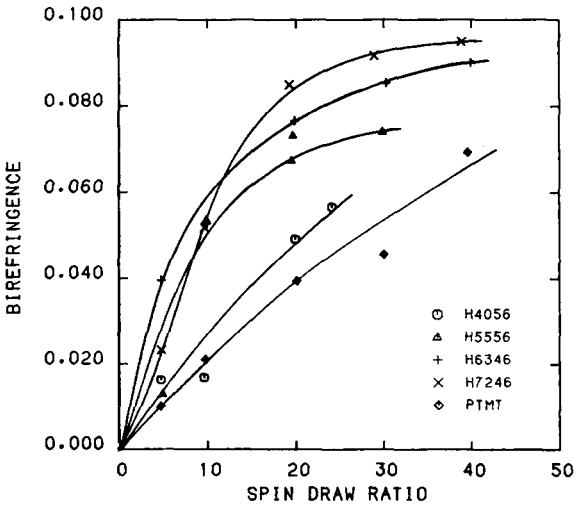

Fig. 13. Birefringence of the as-spun filaments as a function of composition and spin draw ratio.

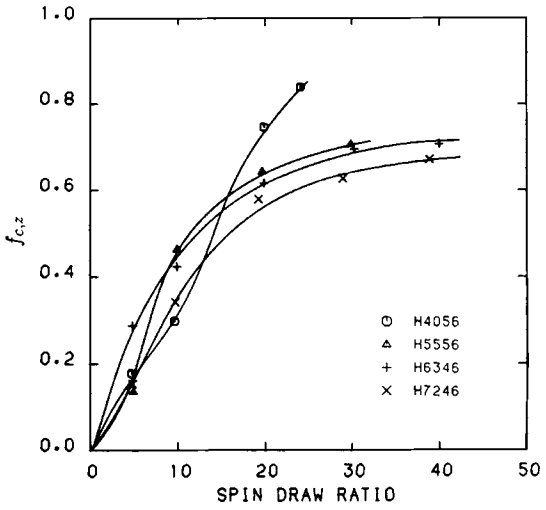

Fig. 14. Crystalline orientation functions $f_{c,z}$ of the as-spun filaments as a function of composition and spin draw ratio.

As was shown in Figure 10, these copolymers may not be completely above their glass transition region at room temperature (25°C). Thus, any amorphous orientation created during spinning may be partially "frozen in." Immersion in boiling water would be expected to raise the temperature of the as-spun filaments to a point well above their T_g, allowing the amorphous regions to relax. The shrinkage in boiling water was used as a rough measure of the amorphous orientation in these filaments. Shrinkage values are given in Table III. None of the as-spun filaments show any significant shrinkage, except for those spun from H4056 and 200 and 250 m/min. In fact, some of the filaments expand by 1 or 2%, probably as a result of further crystallization. Thus, these filaments possess little or no preferred amorphous orientation. The H4056 filaments spun at 200 and 250 m/min were drawn 18% and 32%, respectively, between the two take-up godets during spinning to prevent sagging in the spinline. This most likely created a strain in the amorphous phase as the samples were solidifying, resulting in a significant level of amorphous orientation.

TABLE III
Percent Shrinkage of As-Spun filaments After Immersion in Boiling Water

Sample	50	100	200	250	300
H4056	−0.9	−0.5	8	14	—
H5556	−0.1	—	—	—	0.9
H6346	−2.6	—	—	—	0.4
H7246	−1.6	—	—	—	−2.0
PTMT	−1.8	—	—	—	−2.2

Note: The take-up velocity in m/min is shown at the top of each column. Negative values reflect an increase in length.

TABLE IV
Degree of Phase Separation w_c of As-Spun Filaments as a Function of Composition and Spinning Speed

Sample	50	100	200	250	300	400
H4056	0.68	0.68	0.68	0.68	—	—
H5556	0.61	—	—	—	0.61	—
H6346	0.41	—	—	—	0.41	—
H7246	0.30	0.29	0.30	—	0.29	0.29
PTMT	0.00	—	—	—	0.00	—

Note: The take-up velocity in m/min is shown at the top of each column.

Degree of Phase Separation

The degree of phase separation is one of the most important parameters in determining the physical and mechanical behavior of these copolymers since it determines the degree of physical crosslinking and the glass transition temperature for a given sample. Changes in the degree of phase separation were followed by measuring changes in bulk density and small angle x-ray scattering power. The quantities ϵ and w_c as determined from SAXS and density techniques, respectively, are useful in comparing the relative degrees of phase separation among the different copolymer samples. The results of these experiments are shown in Table IV and Figure 15. Except for the H4056 filament spun at 250 m/min, neither w_c nor ϵ show much change with SDR, indicating that the DPS is virtually independent of this parameter. There is, however, a large effect of composition on the DPS: the DPS decreases as HSC increases. Filaments spun from PTMT were essentially amorphous. This is in spite of the fact that during the isothermal crystallization studies, the crystallization rate increased as HSC increased (at a given degree of supercooling).

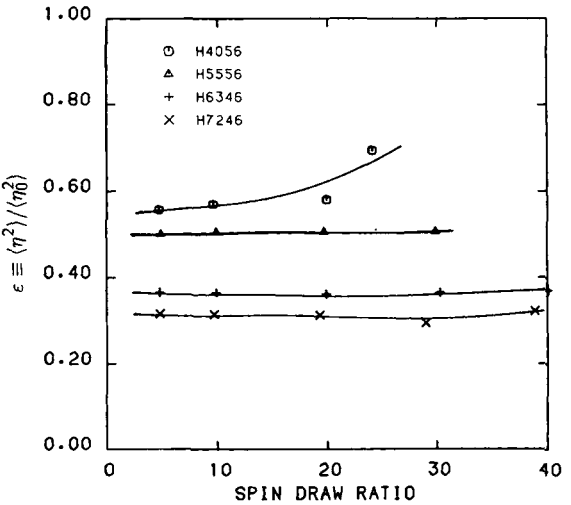

Fig. 15. Relative degree of phase separation ϵ for each composition as a function of spin draw ratio.

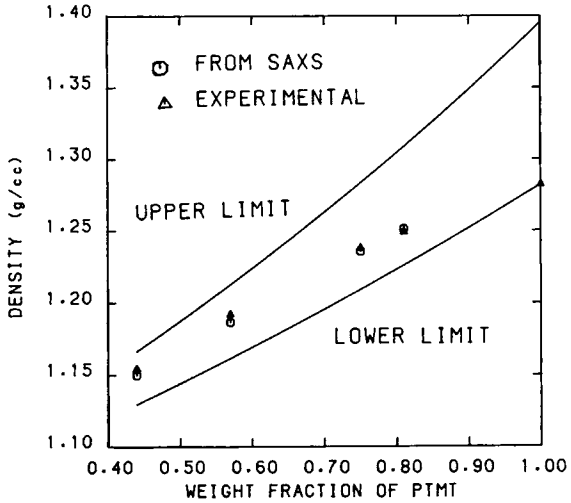

Fig. 16. Comparison of measured densities and those calculated from SAXS data using eq. (10). The theoretical upper and lower limits of density were calculated with the assumption that no crystallization of the soft segments occurs.

There is good agreement between measured density values and those calculated from SAXS data by substituting ϵ for w_c in Eq. (10). The density values, as well as the upper and lower theoretical limits of density for these compositions, are shown in Figure 16. The DPS approached 100% as the density approaches the upper limit for a given composition. The DPS, however, is only a measure of the fraction of maximum crystallinity that a particular composition can obtain and does not indicate absolute crystallinity. To determine the degree of crystallinity, both the HSC and DPS must be taken into account:

$$x_c = \varepsilon \omega_1 \tag{15}$$

or

$$x_c = w_c \omega_1 \tag{16}$$

The results of these calculations are shown in Figure 17. The degree of crystallinity in the copolymer filaments ranges from 25 to 35%. In contrast to the DPS, the absolute crystallinity exhibits a maximum with respect to composition.

Discussion of Structure

Air quenching produced opaque or translucent filaments depending on the composition and take-up velocity. Spinning into a quench bath produced translucent filaments under all the conditions investigated. Thus, it is believed that water quenching produces a higher nucleation density and smaller morphological features than does the slower air cooling.

The WAXD and rheovibron results indicate that the copolymer filaments have a two phase structure as has been reported for other copolyester samples

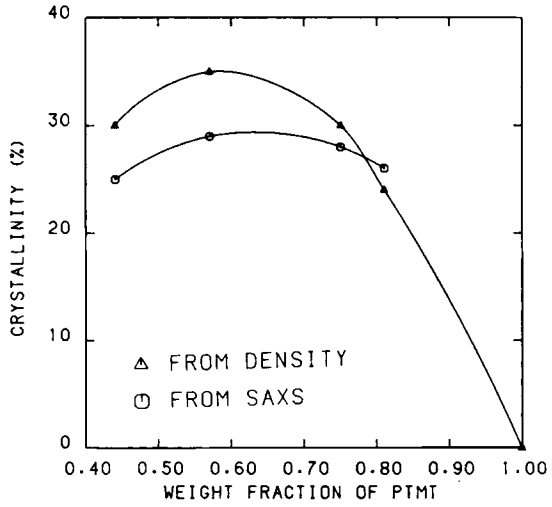

Fig. 17. The degree of crystallinity of as-spun filaments as a function of composition. There is little or no variation of crystallinity with spin draw ratio.

processed in different ways by other investigators.[3,4,27] One phase consists entirely of crystalline PTMT segments, while the other phase is a mixture of uncrystallized hard segments and PTMEG-T.

The PTMT filaments obtained by spinning into water are amorphous. Since the copolymer filaments are quenched under the same conditions, and since the crystallization rate has been shown to decrease as HSC decreases, it is unlikely that much crystallization of the PTMT segments can occur before the filaments reach the quench temperature. Also, the long period and the degree of phase separation are virtually independent of SDR for a given composition, so crystallization appears to occur at the same temperature and to the same extent regardless of take-up velocity. For these reasons it is believed that most if not all of the crystallization takes place after quenching. "Stress-induced crystallization" does not appear to significantly enhance the crystallization rate in these copolymers under these spinning conditions.

The degree of phase separation in the quenched filaments was found to decrease as HSC increased. One explanation for this may be that because of its sluggish crystallization kinetics, the H4056 composition crystallizes slowly at the bath temperature and has very low crystallinity as it emerges from the bath. Its low T_g, however, allows it to continue to crystallize after spinning so that it eventually reaches a relatively high level of phase separation. As hard segment content increases, the crystallization rate at a given degree of undercooling increases. But the glass transition temperature also increases and, at the bath temperature, the mobility of the uncrystallized hard segments is reduced as HSC increases. This limits the amount of phase separation that can take place at the quench temperature (or afterwards at room temperature). This does not necessarily mean lower crystallinity though. The absolute degree of crystallinity depends on both the amount of the crystallizable component (HSC) and its degree of transformation (DPS). As a result, there is a maximum in crystallinity with respect to composition. This maximum occurs near the H5556 composition. The reasonable rapid crystallization and relatively high

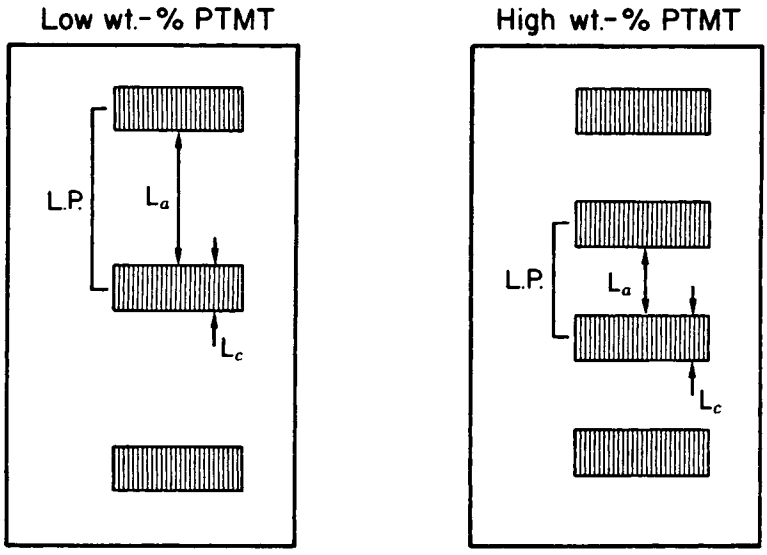

Fig. 18. Model of the domain structure explaining the effect of composition on the long period. L_c is the thickness of the crystallites while L_a is the distance between adjacent crystallites.

level of crystallinity reached by the H5556 filaments near the quench temperature help explain why this composition is the easiest to spin.

The long periods of the copolymer filaments were found to increase sharply as HSC decreased. In homopolymers, changes in long period are usually associated with changes in lamellar thickness. This phenomenon, however, cannot explain the behavior of the copolymer filaments. Measurements of the line breadth of the $(\bar{1}04)$ diffraction peaks indicate that the thickness of the crystallites do not change much with composition. Thus, the large increase in long period with decreasing HSC is due largely to an increase in the distance between crystalline domains in the axial direction as illustrated in Figure 18.

X-ray and birefringence results show that the crystalline chains become increasingly aligned parallel to the fiber axis as SDR is increased. Spinning speeds higher than about 400 m/min were not possible with the water bath due to filament breakage. However, higher spinning speeds probably would not produce appreciably higher levels of orientation judging from the way f_c and the birefringence begin to level off at take-up velocities of around 300 to 400 m/min. Similar copolyester-ether filaments spun by Abhiraman et al.[12] using a water bath showed no significant increase in birefringence upon increasing the take-up velocity from 500 to 1000 m/min (SDRs of about 50–110).

The shrinkage results show that, except for the two H4056 filaments that were drawn slightly, large levels of amorphous orientation are not produced by this spinning technique in any of the copolymer filaments, even at high spin draw ratios. Thus, the technique of melt spinning into a water quench bath can be used to produce copolyester-ether filaments having a high level of crystalline orientation while maintaining a fairly low level of amorphous orientation. These features are desirable for high strength and elastic recovery.

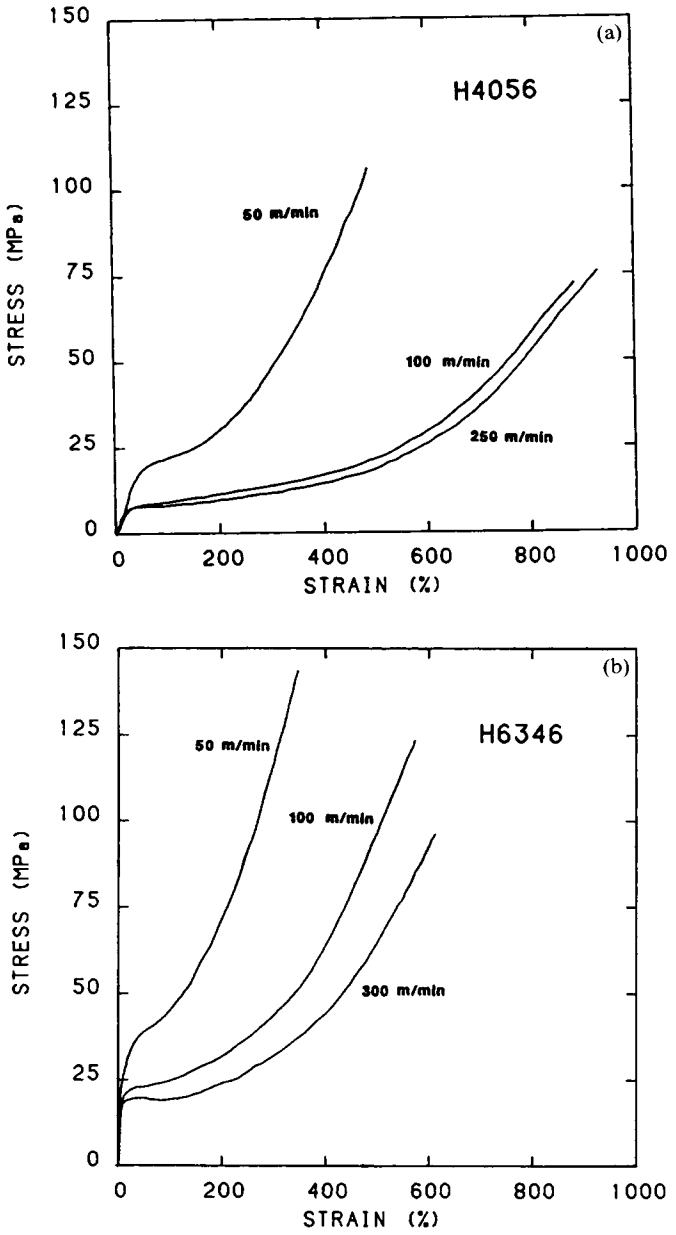

Fig. 19. Effect of increasing take-up velocity on the stress-strain curves for (a) H4056 filaments and (b) H6346 filaments.

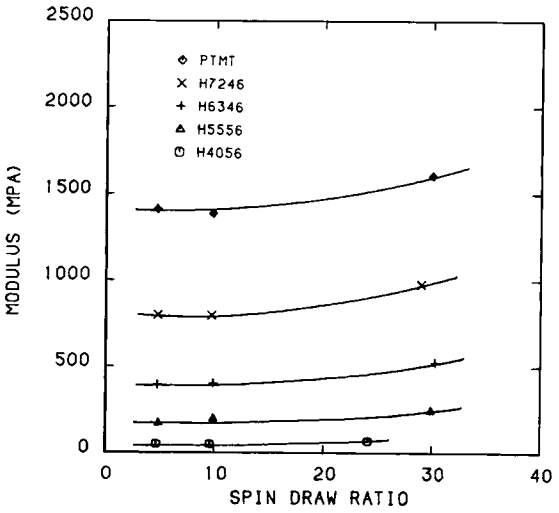

Fig. 20. Modulus of the as-spun filaments as a function of spin draw ratio and composition.

MECHANICAL PROPERTIES

Tensile Properties

The effect of spin-draw ratio and composition on the stress–strain behavior of the copolymer filaments can be seen in Figure 19. The tensile properties of the as-spun filaments were determined from such curves and are discussed in the following sections.

The general stress–strain behavior of isotropic copolyester-ethers has been previously interpreted by Cella.[4] The high initial modulus of these copolymers as compared with conventional crosslinked elastomers is attributed to the pseudoelastic deformation of the crystalline network. Above about 25% elongation the material draws as the crystalline matrix is irreversibly deformed. At high elongations the material behaves similarly to crosslinked elastomers as the stress is increasingly borne by the continuous elastomeric phase. These general relationships should be useful in interpreting the tensile properties of the melt-spun filaments.

Initial Modulus. The moduli of the as-spun filaments are shown as a function of SDR and composition in Figure 20. The modulus increases slightly with increasing SDR as a result of the higher levels of hard segment orientation, but this appears to be a second-order effect. The modulus increases greatly, however, as the HSC increases. This is not surprising considering the modulus of PTMT is much higher than that of PTMEG.

Elongation to Break. Elongations to break from about 700 to 950% were observed for filaments spun at low speed, depending on the composition. These compare with values of 250 to 450% reported for films.[28] The ultimate elongation of the as-spun filaments drops as SDR increases. This is directly related to the increase in the crystalline chain orientation (f_c) as shown in Figure 21. The PTMT filaments remain amorphous and show less dependence

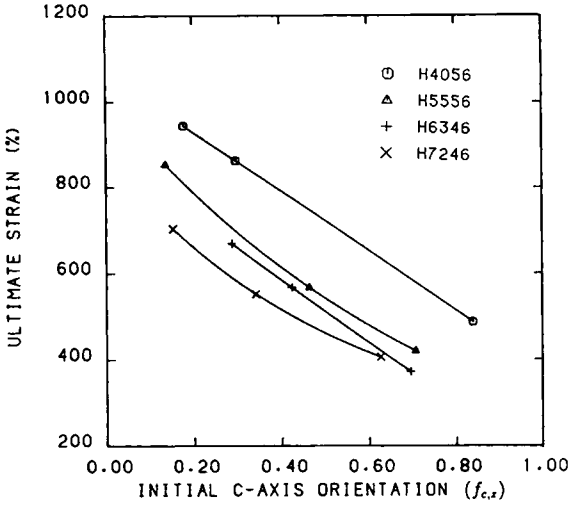

Fig. 21. Ultimate strain as a function of composition and crystalline orientation.

on SDR. Stress-strain curves of PTMT filaments at all SDRs show a considerable amount of necking and drawing behavior. Figure 21 also shows that the ultimate elongation increases as HSC decreases for a given value of f_c. This is due to the increase in the weight fraction of highly coiled amorphous chains as HSC decreases.

Tenacity. Tenacities in the range of about 70 to 150 MPa were measured for the copolymer filaments depending on composition. Abhiraman[12] has reported values of around 50–125 MPa for PTMT/PEO filaments that were 45–50 wt% PTMT. Unoriented films of PTMT/PTMEG-T have tenacities of only about 25–40 MPa.[28] For comparison, elastic filaments of polypropylene have been reported with tenacities of 100–450 MPa[29] and polyester fibers produced by high speed spinning have tenacities in the range of 100–600 MPa.[30]

The tenacity of the unannealed copolymer samples increases with increasing HSC and increasing initial crystallite orientation as shown in Figure 22. The higher initial orientation results in more chains being aligned in the fiber axis direction at high elongations, increasing the fiber strength. Tenacity increases with increasing hard segment content.

Elastic Properties

The elastic properties of the filaments were investigated by subjecting samples to cyclic testing on an Instron tensile tester. The strain recovery and work recovery at each elongation were calculated from the extension and retraction curves as previously described. The work recovery is always lower than the strain recovery, since the latter is only a measure of dimensional changes and does not take into account the retractive force. The energy losses are associated with plastic deformation of the crystalline domains and hysteresis. The hysteresis is due to reorientation of crystallites and viscoelastic effects in the amorphous phase.

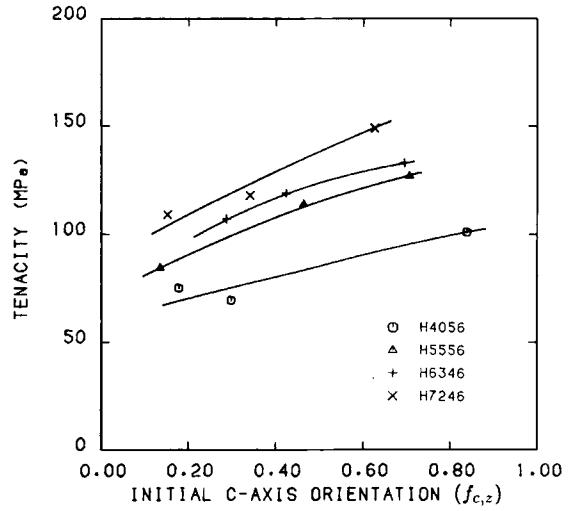

Fig. 22. Tenacity as a function of composition and crystalline orientation.

The effect of SDR on the strain recovery of H4056 and H7246 filaments can be seen in Figure 23. Increasing the SDR produces higher levels of crystallite orientation and results in higher strain recovery at low elongations. As f_c is increased, there is less tendency for the crystallites to reorient at low elongations and they are more resistant to plastic deformation. The higher DPS and greater fraction of PTMEG in the H4056 filaments results in superior elastic properties compared to the H7246 filaments. The elastic performance of the highly oriented H7246 filament approaches that of the H4056 filaments at very low elongations, (< 5%), but plastic deformation of the crystallites

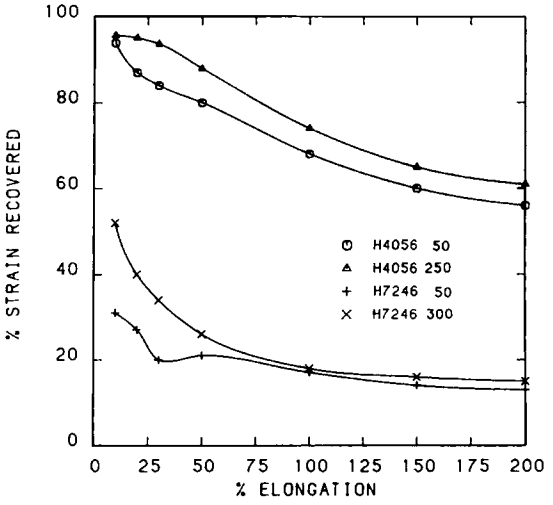

Fig. 23. Strain recovery of H4056 and H7246 filaments spun at low (50 m/min) and high (250–300 m/min) take-up velocities.

prevents the H7246 filaments from achieving high elastic recovery at higher elongations.

CONCLUSIONS

The crystallization rate of the copolyester-ethers was found to decrease with decreasing HSC at constant undercooling. When cooling from the melt at constant rate, the crystallization temperature decreases as HSC decreases and as cooling rate increases. When quenched in liquid nitrogen, either very small crystallites are formed or the degree of crystallinity is very small. Further crystallization may take place in the quenched samples when they are warmed to room temperature.

These copolymers are difficult to spin because of their elastic nature and sluggish crystallization kinetics. In crystallizable homopolymers, the crystallization rate is usually increased by several orders of magnitude at higher spinning speeds by a "stress induced crystallization" mechanism. However, the elastic nature of the copolymer filaments causes melt instabilities that prevent them from being spun at speeds much higher than about 2000 m/min in air. These speeds are apparently not high enough for stress-induced crystallization to play a major role in the crystallization behavior. When spinning at low speeds, the filaments low in HSC do not crystallize on-line and are too tacky and soft to be taken up with a conventional constant tension winder. Spinning into a water bath causes the filaments to solidify sufficiently before winding to eliminate the sticking problem.

The H7246 and H6346 filaments crystallize enough in the water bath that they may be taken-up, but they are still "soft" at this point. Care must be taken not to stretch them in this state or significant amorphous orientation will result. These two compositions crystallize further after take-up. The H5556 composition appears to crystallize most rapidly in the water bath and reaches the highest level of crystallinity. Filaments from this composition are solid and reasonable strong immediately after emerging from the bath and, consequently, are the easiest to spin. They do not appear to crystallize much further after take-up. The H4056 composition crystallizes very little in the bath, but because of its low glass transition temperature it is able to crystallize at room temperature and eventually reaches a high degree of phase separation. Birefringence measurements show that primary crystallization continues in this composition for up to ten minutes after spinning. The H4056 filaments stretch very easily in a "taffy-like" manner during the first several minutes after spinning.

WAXD and rheovibron results indicate that a two-phase structure is produced in the copolymer filaments by melt spinning. There is no evidence of a crystalline soft segment phase in any of the compositions. SAXS patterns indicate that lamellar-like crystallites are formed which become preferentially oriented perpendicular to the fiber axis at high spin draw ratios. As HSC content decreases the lamellae become more widely spaced.

Density and SAXS results indicate that almost two-thirds of the hard segments in the H4056 filaments have crystallized after conditioning at room temperature. This amounts to about 30% crystallinity as calculated from

density. As HSC increases, the DPS decreases. In the H7246 filaments, less than one-third of the hard segments crystallize, corresponding to a crystallinity of about 24%. In contrast to the DPS, there is a maximum in crystallinity with respect to composition: the H5556 filaments reach about 35% crystallinity. Apparently, the H5556 composition is nearer its optimum crystallization temperature in the bath than either H7246 or H6346. The DPS of the water quenched filaments does not change much with SDR, indicating that stress induced crystallization does not greatly enhance the crystallization rate within the range of spinning conditions explored in this research.

High levels of crystalline orientation can be produced at spinning speeds as low as 250 to 300 m/min using the water quench technique. If care is taken so that the filament is not drawn during take-up, the amorphous orientation remains quite low.

The structural features desired for high elastic recovery include high DPS, high crystalline orientation, and low amorphous orientation. Furthermore, the lamellae should be oriented perpendicular to the fiber axis so that the crystalline chains are parallel to the fiber axis. The amorphous chains should be highly coiled and provide a high level of connectivity between the hard segment domains which anchor the structure.[12] Thus, the water quenched filaments spun at high spin draw ratios have many of the structural features necessary for high elastic recovery.

Both tensile and elastic properties of these filaments were investigated. The modulus is not very sensitive to SDR and crystalline orientation, but increases greatly as HSC increases. The elongation to break and tenacity are highly dependent on the crystalline orientation. Tenacity increases modestly as HSC increases, while ultimate elongation decreases.

Plastic deformation of hard segments during stretching, and hysteresis effects prevent the filaments from exhibiting ideal elastic behavior. The elastic recovery increases greatly as HSC is reduced and to a lesser extent as the crystalline orientation is increased. Both changes act to reduce the amount of plastic deformation in the crystalline phase. The elastic recovery of these filaments can be further enhanced by annealing, but that is the subject of another paper.

References

1. U. Bandara and M. Droscher, *Colloid Polym. Sci.*, **261**, 26–39 (1983).
2. R. M. Briber and E. L. Thomas, *Polymer*, **26**, 8–16 (1985).
3. W. H. Buck, R. J. Cella, Jr., E. K. Gladding and J. R. Wolfe, Jr., *J. Polym. Sci. Polym. Symp.*, **48**, 47–60 (1974).
4. R. J. Cella, *J. Polym. Sci.*, **42**, 727–740 (1973); *Encycl. Polym. Sci. Technol.*, **2** (Suppl.) 485–510 (1977).
5. Abdul Ghaffar, Isaac Goodman, and Ivan Hall, *Br. Polym. J.*, **5**, 315–325 (1973).
6. A. Lilaonitkul, J. West, and S. L. Cooper, *J. Macromol. Sci Phys.*, **B12**(4), 563–597 (1976).
7. A. Lilaonitkul and S. L. Cooper, *Rubb. Chem. Technol.*, **50**(1), 1–23 (1977).
8. A. Lilaonitkul and S. L. Cooper, *Macromolecules*, **12**(8), 1146–1156 (1979).
9. R. W. Seymour, G. M. Estes, and S. L. Cooper, *Macromolecules*, **3**, 579 (1970).
10. R. W. Seymour, J. R. Overton, and L. S. Corley, *Macromolecules*, **8**(3), 331–335 (1975).
11. G. Wegner, T. Fujii, W. Meyer, and G. Lieser, *Die Angew. Makromol Chem.*, **74**, 295–316 (1978).

12. A. S. Abhiraman, Y. M. Kim, and K. P Wagener, *J. Polym. Sci. Polym. Phys. Ed.*, **25**, 205–228 (1987).
13. C. M. Boussias, R. H. Peters, and R. H. Still, *J. Appl. Polym. Sci.*, **25**, 869–878 (1980).
14. L. Zhu and G. Wegner, *Macromol. Chem.*, **182**, 3625–3638 (1981).
15. F. A. Bovey, *Pure Appl. Chem.*, **54**(3), 559–568 (1982).
16. L. W. Jelinski, F. C. Schilling, and F. A. Bovey, *Macromolecules*, **14**, 581–586 (1981).
17. J. W. Van Bogart, A. Lilaonitkul, and S. L. Cooper, *Adv. Chem. Series*, **176**, 4–29 (1979).
18. R. E. Wetton and G. Allen, *Polymer*, **7**, 331–365 (1966).
19. N. Yoshihara, A. Fukushima, Y. Watanabe, A. Nakai, S. Nomura, and H. Kawai, *Sen-I Gakkaishi*, **37**(10), T-387–T-413 (1981).
20. O. Glatter and O. Kratky, *Small Angle X-ray Scattering*, Academic Press, New York, 1982.
21. R. J. Matyi and B. Crist, Jr., *J. Polym. Sci. Polym. Phys. Ed.*, **16**, 1329–1354 (1978).
22. R. Bonart and E. H. Müller, *J. Macromol. Sci. Phys. Ed.*, **10**, 177 (1974).
23. J. T. Koberstein and R. S. Stein, *J. Polym. Sci. Polym. Phys. Ed.*, **21**, 1439–1472 (1983).
24. J. C. Stevenson and S. L. Cooper, *J. Poly. Sci. Polym. Phys. Ed.*, **26**, 953–966, (1988).
25. M. Avrami, *J. Chem. Phys.*, **9**, 177 (1941).
26. L. Zhu, G. Wegner, and U. Bandara, *Macromol. Chem.*, **182**, 3639–3651 (1981).
27. W. K. Witsiepe, *Adv. Chem. Ser.*, **129**, 39–60 (1973).
28. G. Zaiser, *Plastics Eng.*, **34**(5), 61–64 (1978).
29. R. J. Samuels, *J. Polym. Sci. Polym. Phys. Ed.*, **17**, 535–568 (1979).
30. J. Shimizu, *Sen-i Gakkaishi*, **33**(5), 1977.

Accepted August 9, 1989